Materials Chemistry and Physics 258 (2021) 123921

Contents lists available at ScienceDirect

Materials Chemistry and Physics

journal homepage: www.elsevier.com/locate/matchemphys

Effects of synthesis and sintering temperature in BCT-BST ceramics

C. Pavithra [a], W. Madhuri [b,*], S. Roopas Kiran [c]

[a] Department of Physics, Marudhar Kesari Jain College for Women, Vaniyambadi, Tamilnadu, India
[b] Ceramic Composites Laboratory, CCG, VIT, Vellore, Tamilnadu, 632014, India
[c] Department of Physics, VIT, Amarvathi, Andhra Pradesh, India

HIGHLIGHTS

- 0.55($Ba_{0.9}Ca_{0.1}$)TiO_3-0.45Ba($Sn_{0.2}Ti_{0.8}$)O_3 (BCT-BST) is prepared by three different methods.
- Densification temperature varies between 1250 °C and 1400 °C depending on the synthesis technique.
- The high dielectric constant is achieved around 18 K.
- The phase transition is noticed around 71 °C at all the preparation methods.
- BCT-BST is a soft ferroelectric material.

ARTICLE INFO

Keywords:
BCT-BST
Solid state method
A sol-gel method
Molten-salt method
High dielectric constant

ABSTRACT

Morphology and properties of ceramics are first attributes of synthesis techniques and sitering temperature. In order to understand the effect of synthesis techniques and sintering temperature 0.55($Ba_{0.9}Ca_{0.1}$)TiO_3-0.45Ba($Sn_{0.2}Ti_{0.8}$)O_3(BCT-BST) is synthesized by solid state reaction (SSR), sol-gel method and molten-salt methods. The cubic crystal structure of all the synthesized BCT-BST is confirmed by X-ray powder diffraction analysis. Densification temperature varies between 1250 °C and 1400 °C depending on the synthesis technique. The morphology and particle size of each of BCT-BST is studied using scanning electron microscope. Particle size is found to be in the range of 32 nm–60 nm. Dielectric studies on each of BCT-BST are carried out as a function of temperature and frequency. The morphotropic phase boundary is noticed at 71 °C and a high dielectric constant of 18,000 noticed for sol gel synthesized BCT-BST. A soft ferroelectric hysteresis curve is exhibited by each of BCT-BST.

1. Introduction

Ferroelectric ceramics have wide range of applications in the electronics industry because of its high dielectric constant, piezoelectric and ferroelectric property [1,2]. Of all lead based ceramics especially PZT offer excellent dielectric and ferroelectric as well as piezoelectric properties best suited for various applications. Lead-based materials find their place in the electronic and microelectronicdevices such as non-volatile memory devices, sensors, capacitors, actuators, microelectronic mechanical systems (MEMS) etc. However, such lead-based materials face high volatilization and pose environmental hazards, due to toxic nature of lead. In the given scenario there is an urgent need to develop lead-free materials with colossal dielectric constant and giant d33 [3,4]. Barium titanate offers good dielectric and ferroelectric properties and is environment friendly. With high dielectric constant and ferro/piezoelectric coefficient barium titanate (BT) is a potential candidate that can replace PZT. Further improvement in BT is desirable and the contemporary research is stirring in the direction [5]. The basic ways to improve ferroelectric properties is to decrease the grain size so as to increase surface to volume ratio. Large grain surface favours large local fields resulting in improved dielectric constant. Another way is at phase boundary points, at these points dipoles are unstable and align in the applied direction resulting in high dielectric constant [5–7]. The method of phase boundary modification is done by partial replacement of barium in the ceramics. On rigorous literature survey [8] it is noticed that BCT-BST ceramic is reported to exhibit giant dielectric constant and very high d33 coefficient. Further the properties of ceramic depends on the method of synthesis and the temperature it is sintered. Adopting a

* Corresponding author.
E-mail address: madhuriw12@gmail.com (W. Madhuri).

https://doi.org/10.1016/j.matchemphys.2020.123921
Received 20 August 2020; Received in revised form 5 October 2020; Accepted 11 October 2020
Available online 26 October 2020

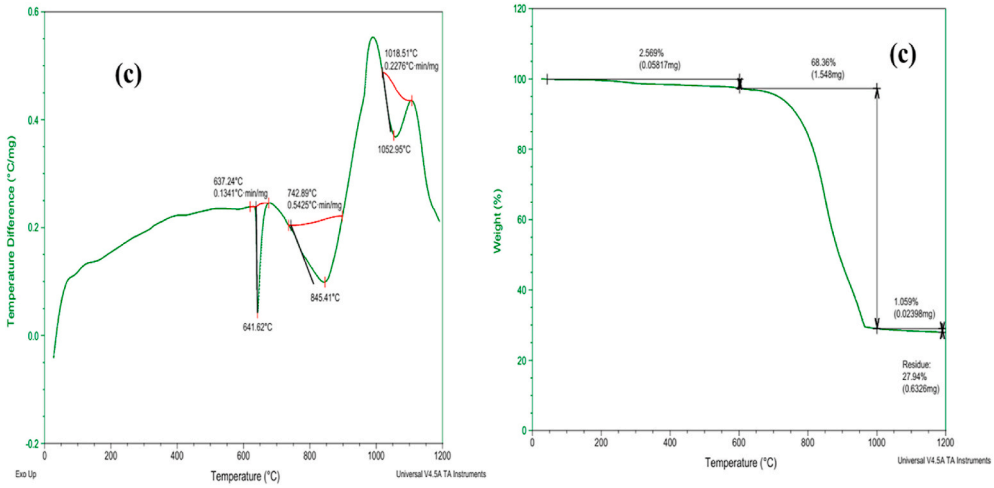

Fig. 1. Thermal analysis of BCT-BST (a) SSR (b) sol-gel method and (c) molten-salt method.

Table 1
Sintering condition of the composites.

Synthesis Technique	Calcination Temperature (°C)	Sintering Temperature (°C)
SSR	1300	1450
Sol-gel Method	1000	1250
Molten-salt Method	1000	1225

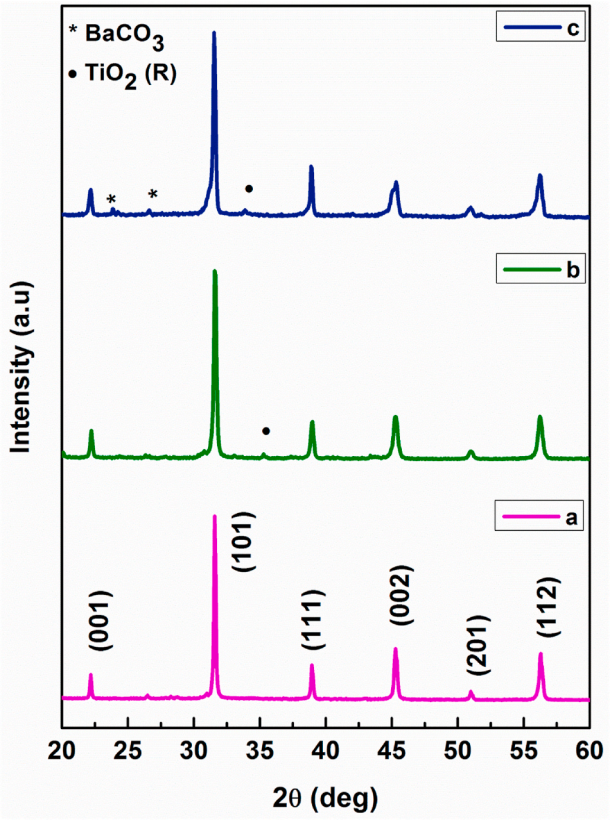

Fig. 2. XRPD pattern of BCT-BST (a) SSR (b) Sol-Gel Method and (c) Molten-Salt Method.

suitable synthesis technique and sintering temperature can improve/-fine tune the characteristics of ceramics. When compared with conventional solid state techniques, chemical routes have advantages like homogeneous, pure, and uniform nano particle yield. While the conventional solid state reaction (SSR) mostly yields micro particles wet route synthesis ensures nanoparticles. Further the required sintering temperature for wet route is less than that of SSR [1,8,9]. The present article details the comparative study of structural, dielectric and ferroelectric properties of BCT-BST ceramics synthesized by solid state reaction, sol-gel method and molten-salt method.

2. Experimental details

2.1. Solid state reaction

Barium carbonate (BaCO3, Sdfine99.0%), calcium carbonate (CaCO3, Alfa Aesar99%), stannic oxide (SnO2, Alfa Aesar99.5%) and titanium dioxide (TiO2, Alfa Aesar99.0%) were used as raw materials. The starting materials are taken in stoichiometric ratio and grinded in an agate mortar with ethanol then the sample is transferred into tungsten jar (the sample and ball ratio is 1:10) and the sample is grinded for 6 h in Fritsch planetary mono mill after that the sample is calcined at 1300 °C for 4 h using conventional furnace. The resultant powder is compacted and sintered using microwave furnace at 1400 °C for 30 min. The sample is made into a pellet in 1 cm diameter dye using PVA as a binder, and then sintered. The sintered pellet is used to measure the dielectric measurements. The pellet is pasted with silver paint on both surfaces for good ohmic contact.

2.2. SOL-GEL synthesis procedure

The starting materials are barium acetate (BaC4H6O4 Sigma-Aldrich, 99%), calcium nitrate (Ca(NO3)2 4H2O, Sigma-Aldrich, 99%), tin chloride (SnCl4·5H2O, Sigma-Aldrich, 99%), and titanium butoxide (Ti(OC4H9)4, Sigma-Aldrich, 99%) are taken in stoichiometric ratio. Initially, barium acetate is mixed with glacial acetic acid and stirred continuously. Calcium nitrate and stannic chloride tin chloride are separately stirred in ethanol to make two different solutions. All these three solutions are mixed together and continued stirring for 30 min. Then titanium butoxide is added to the solution drop by drop. The prepared solution under continuous stirring is dehydrated at 100 °C for 4 h. The obtained whitegel is dried to obtain the powder. The prepared powder is calcined at 1000 °C and sintered at 1250 °C using microwave

Table 2
Physical properties of BCT-BST composites.

Synthesis methods	ρ_B (g/cm^2)	ρ_{th} (g/cm^2)	P	Crystallite Size in nm (XRPD)	Particle size in nm (SEM)	Scherrer Strain (ε*)	W–H Strain (ε)
SSR	5.75	5.771	0.0379	50	60	0.1388	0.1327
Sol-gel	5.72	5.742	0.0384	35	32	0.1889	0.1708
Molten-salt	5.73	5.748	0.0313	35	45	0.2110	0.2241

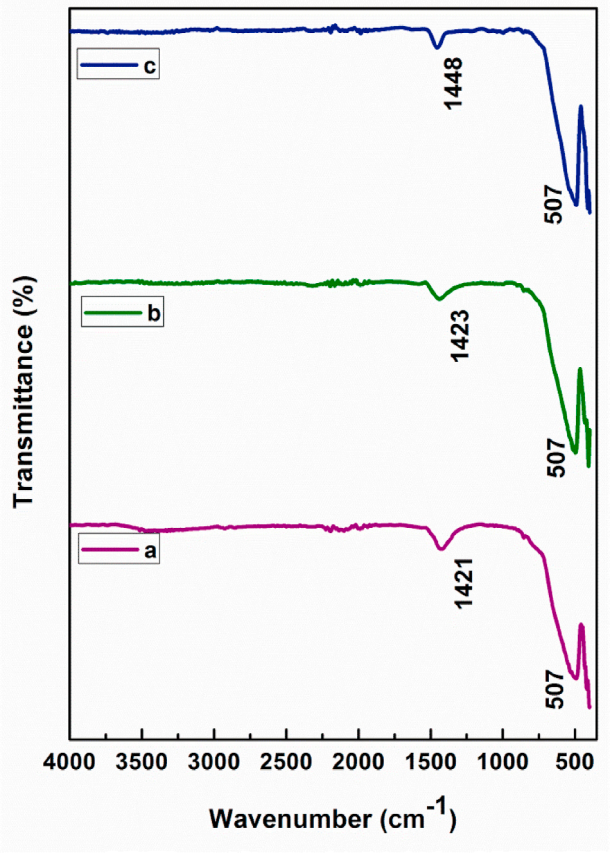

Fig. 3. FT-IR spectra of BCT-BST (a) SSR (b) sol-gel method and (c) molten-salt method.

furnace.

2.3. MOLTEN-SALT synthesis procedure

Barium carbonate (BaCO3, Sdfine99.0%), calcium carbonate (CaCO3, Alfa Aesar99%), stannic oxide (SnO2, Alfa Aesar99.5%), titanium dioxide (TiO2, Alfa Aesar 99%), sodium chloride (NaCl, Sdfine, 98%) and potassium chloride (KCl, Sdfine, 98%) are used as raw materials in stoichiometric ratio. Initially, all the powders are mixed using agate mortar. Sodium chloride and potassium chloride are taken in 1:1 ratio and the mixture is calcined for 1000 °C. The calcined sample is washed for several times using deionized water to remove the salt ions until Cl^- is not detected using $AgNO_3$ solution. The washed powder is heated at 150 °C using hot air oven to obtain the dried powder. The prepared sample is sintered at 1250 °C using microwave furnace.

3. Characterization technique

Thermal analysis of the synthesized compounds is by Thermogravimetric Analysis (SDT Q600 V2 0.9 Build 20). Crystal structure and crystallite size were analyzed by X-ray powder diffraction (XRPD) method using (D8 Advance, Bruker diffractometer). The vibrational bands of the synthesized compounds are analyzed by Fourier Transformation-Infra Red (Shimadzu, IR Affinity-1) analysis in the wavelength range is 4000-400 cm^{-1}. The particle size of the compounds is analyzed using Scanning Electron Microscopy (Carl Zeiss EVO 18). Temperature variation of the conductivity and dielectric constant are obtained by using the LCR Hi TESTER (HIOKI-3532-50). Sample is placed between the electrodes of the computer interfaced oven. The P-E loops of the samples are observed using P-E loop tracer, Marine India.

4. Result and discussion

4.1. Thermal analysis

The thermal analysis of the sample is used to identify the densification temperature of the material. For as-synthesized samples, thermal analysis curves are shown in Fig. 1 from room temperature to 1200 °C, the weight loss and differential thermal analysis is carried out. Fig. 1(a) shows the weight loss of the sample prepared by SSR. The first weight loss is noticed at 208 °C then at 225 °C followed by 430 °C and last at 1092 °C. From room temperature to 208 °C and 225 °C a weight loss of 10% is noticed and it is due to the evaporation of moisture and other wet solvents used during ball milling. The weight loss of about 30% between 400 °C and 650 °C is due to the partial reaction of the carbonate ingredients to form BCT-BST phase [4]. The final weight loss of 12% at 1092 °C will complete the BCT-BST phase formation reaction. The weight loss are in good agreement with the exothermic peaks at 212 °C, 338 °C and 1090 °C in the corresponding differential thermal analysis (DTA) curve. Fig. 1(b) depicts TGA and DTA of BCT-BST prepared via sol-gel technique. Similar to the SSR, three weight loss regions are observed at about 400 °C (2.2%) is attributed to the evaporation or liberation of organic solvents and inorganic compounds/ions like Cl^-. The weight loss of 3.9% at around 700 °C is due to reaction initialization. The reaction forwards and completes the phase formation at 950 °C as no further weight loss is noticed. However the total weight loss observed is only 21%. The DTA for the sample showed a single exothermic peak at 823 °C representing the phase formation around this temperature. Fig. 1(c) shows the sample synthesized via molten salt has shown the maximum weight loss of 68% at 950 °C apart from 2% at 600 °C. This can be again attributed to the complete phase formation and combustion of inorganic salts viz KCl and NaCl respectively. The corresponding exothermic peak are noticed at 641 °C, 845 °C and 1052 °C emphasizing inorganic salt evaporation, reaction initialization and phase formation of BCT-BST respectively [10]. From the above observations a high decomposition is noticed at around 1000 °C for all the samples. Depending on this the samples are calcined at high temperature and further sintered at a temperature greater than the calcination temperature (see Table 1).

4.2. Structural analysis

The phase formation of BCT-BST is studied using X-ray powder diffraction technique (XRPD). Fig. 2 shows the XRPD profile peaks of BCT-BST and all peaks are well matched with the reported literature [8, 11]. The phase formation of BCT-BST exhibits cubic crystal structure. The cubic crystal structure exhibited in the present ceramic is mainly due to the replacement of Ti^{4+} with Sn^{4+} and in good agreement with Zhu et al. Further, $BaCO_3$ impurity phase is noticed at 24° and 27° while TiO_2 rutile phase is noticed at 35° for sol gel and molten salt synthesized

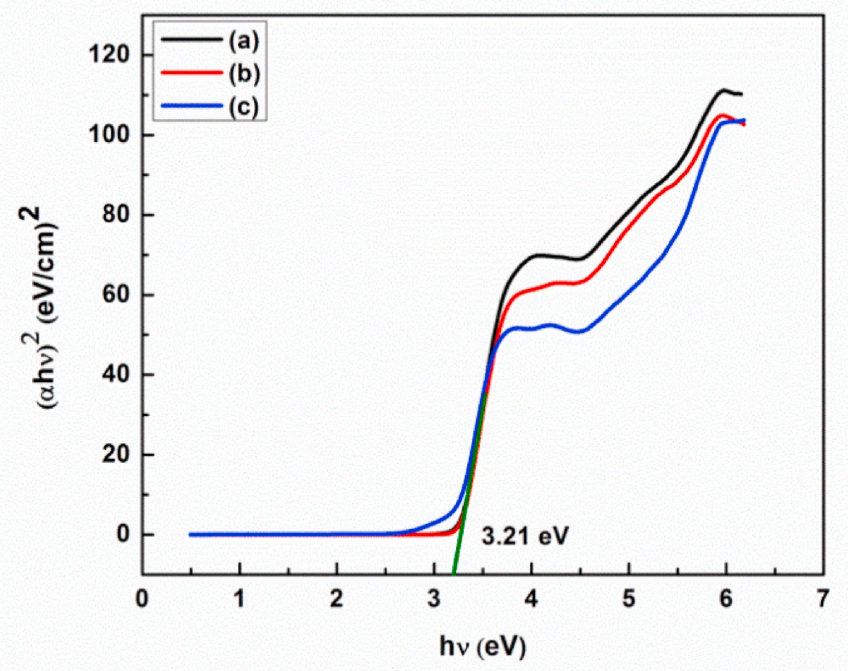

Fig. 4. Tauc plot for BCT-BST (a) SSR (b) sol-gel method and (c) molten-salt method.

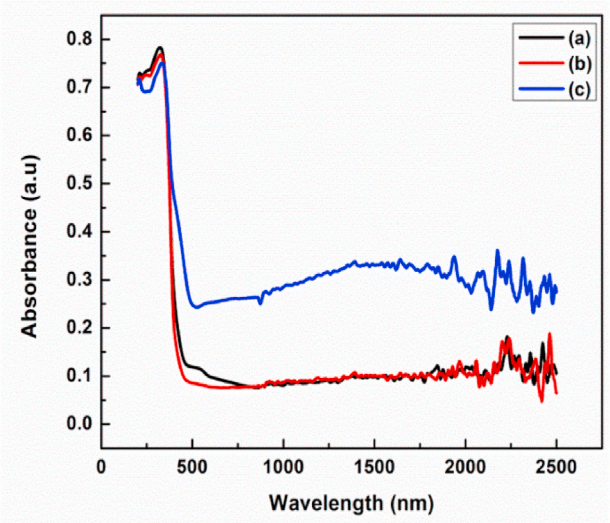

Fig. 5. Absorption spectra for BCT-BST (a) SSR (b) sol-gel method and (c) molten-salt method.

samples. Chemical wet synthesis and lower sintering temperatures adopted in sol gel and molten salt techniques compared to SSR seems to be the reason for these impure phases [12]. The average crystal size is calculated using the Scherrer formula [13]. The density is measured using the density meter. The theoretical density is evaluated from XRPD analysis and are tabulated in Table 2. A very good agreement of porosity (P%) calculated is only 3% for all the ceramics [14]. Densities equal to the theoretical density affirms the estimation of the densification temperature for different synthesis techniques.

4.3. Infrared absorption spectroscopy

The infrared absorption spectroscopy is carried out in the range 4000–400 cm^{-1} wavenumber for the calcined compounds. The vibrational band frequency of the functional groups is below 1000 cm^{-1}. Below 1000 cm^{-1} is fingerprint region of metal oxide bond [15]. Fig. 3 shows the FT-IR spectra of BCT-BST. All the observed peaks are identical and no difference in functional group and metal-oxide vibrational/-stretching mode of the sample is noticed. From this it is concluded that all the synthesis technique has resulted in indistinguishable BCT-BST ceramic formation. The characteristic absorption band of COO^- is usually observed between 1600 and 1200 cm^{-1}. The weak absorption bond around 1400 cm^{-1} is present in all the samples confirming the existence of CO_3^{2-} group construing to the fact that either $BaCO_3$ or $CaCO_3$ or both overlap each other to make a single absorption peak. The colour of the sample also supports to this effect exhibiting colour variation from grey to white for increasing the sintering temperature. The CO_3^{2-} band becomes weaker at high sintering temperatures and is reported to disappear on further increasing the temperatures [16]. The characteristic vibration frequency around 700-400 cm^{-1} is due to metal-oxide bond of Ti–O, BaO, Ca–O and Sn–O.

4.4. Optical property

Fig. 4 shows the Tauc's plot of BCT-BST for all the synthesized compounds. From the plot the estimated energy band gaps of, all the compounds is same value of 3.21 eV. Jyoti et al. also reported a band gap of 3.16 eV for BCT-BZT [2]. Once again it is noticed that the synthesis technique has no influence on the physical, chemical and optical properties of the present compound. Fig. 5 shows the absorption spectra of BCT-BST compounds. Only one absorption band is noticed around 320 nm in all the methods, indicating a UV active window.

4.5. Particle size analysis

Grain size plays a major role in defining the dielectric and ferroelectric properties of these materials. It is found that in BT dielectric permittivity increases with decreasing grain size up to 1 μm below that ε_r decreases rapidly with decreasing grain size [6,17]. In order to study the effect of grain size on various properties of BCT-BST, the morphology is studied using SEM. Fig. 6 shows the SEM images of prepared samples. The particle size is calculated using ImageJ software. The average particle size is found to be around 1 μm, 32 nm and 45 nm for SSR, sol-gel

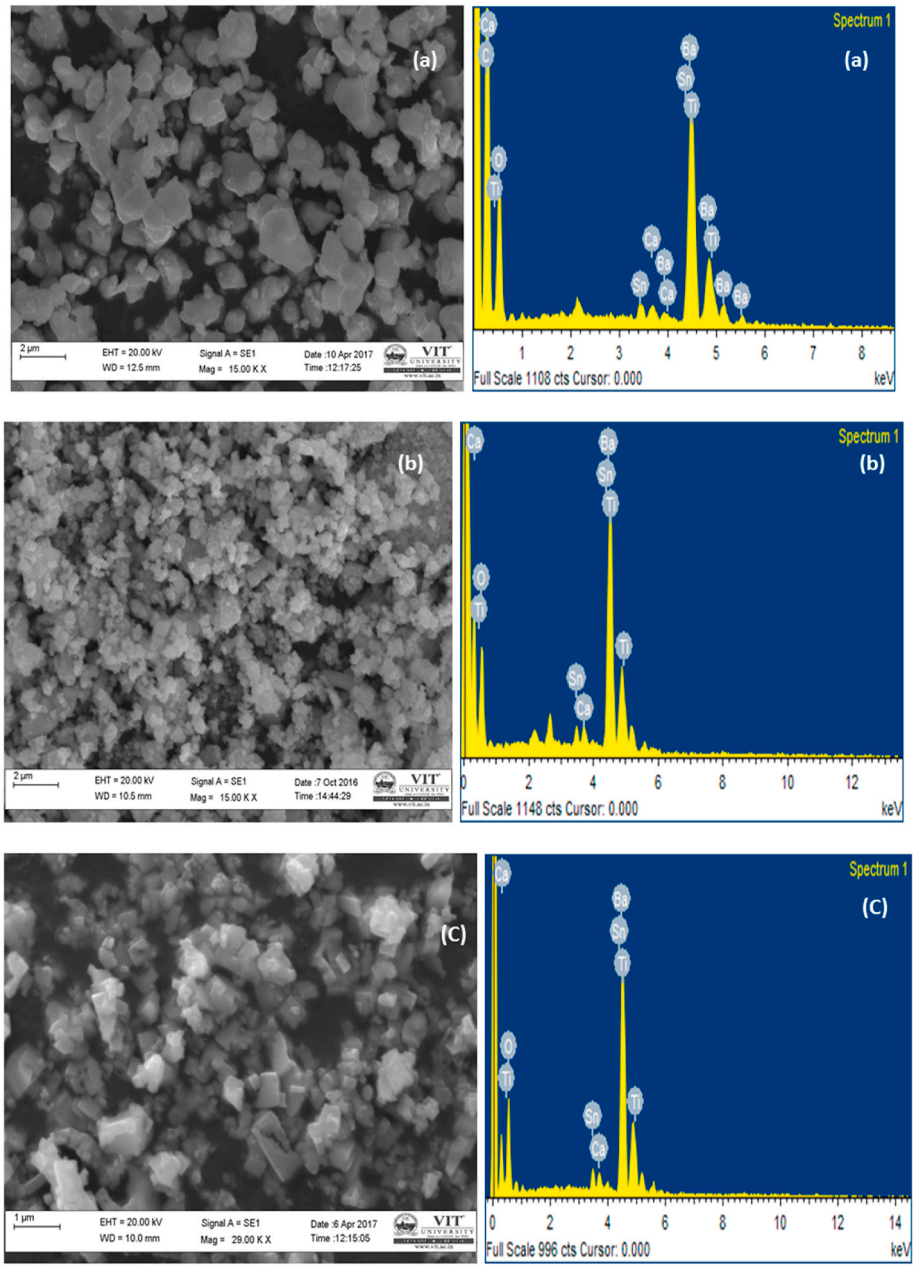

Fig. 6. SEM and EDS of BCT-BST (a) SSR (b) sol-gel method and (c) molten-salt method.

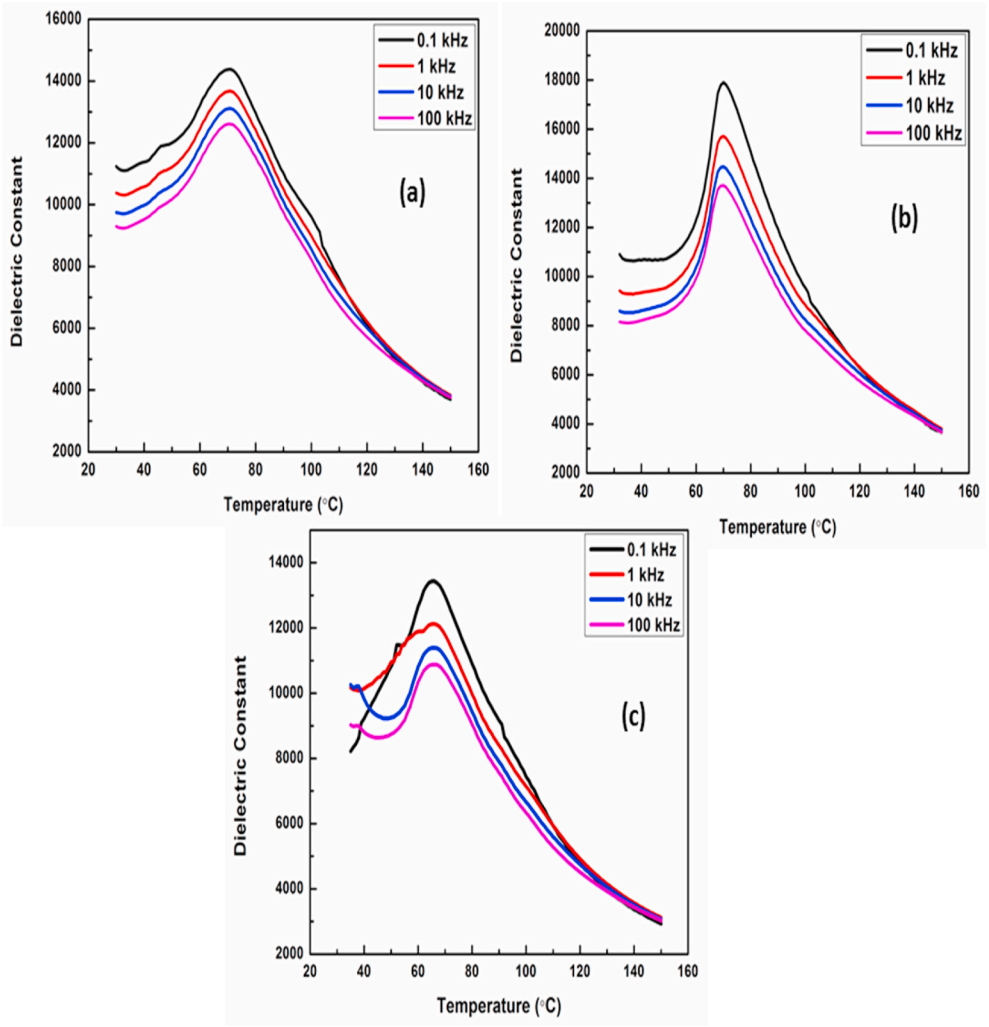

Fig. 7. Temperature with dielectric constant at selected frequency (a) SSR (b) sol-gel method and (c) molten-salt method.

and molten-salt synthesis techniques respectively. It is noticed that the grains seems to grow in three dimensions. However no specific geometry is noticed for SSR and sol-gel samples. The compound synthesized by molten-salt technique has revealed three dimensional block structure [19]. The EDS is shown in Fig. 6 which clearly shows that the presence of elements of the samples.

4.6. Dielectric properties

The dielectric property of the sample is measured as the ratio of real capacitance (C) to geometrical capacitance (C_o) of the sample [18].

$$\varepsilon = \frac{C}{C_O} \tag{1}$$

High dielectric constant is observed in BCT-BST compound. There are intrinsic and extrinsic factors that affect the dielectric constant are grain size, grain boundary, density, internal stress and domain wall motion. Fig. 7 shows the temperature-dependent dielectric constant at various frequencies. On increasing the temperature dielectric constant increases A small hunch noticed near room temperature is attributed to ferroelectric – ferroelectric morphotropic phase transition from orthorhombic to tetragonal and next peak around 70 °C denotes the phase transition, from ferroelectric to para electric and the MPB transition from tetragonal to cubic. Dielectric constant is found to be low at lower temperature and increases with increase in temperature. At low temperature, the dielectric constant is low because of the freezing of the electric dipoles. Though Maxwell Wagner polarization is universal for polycrystalline solids, in the present case dielectric constant is predominantly due to spontaneous polarization of the ferroelectric BCT-BST. On increasing the temperature dielectric constant is also found to increase, and attributed to thermally activated relaxation process rather than thermally driven ferroelectric phase transition. Similar transition was reported by Zhu et al. [8] for BCT-BST compositions prepared by regular ceramic route. The samples SSR and sol-gel method exhibited the phase transition at 71 °C while it is at 66 °C for molten-salt technique. This may be due to the lower sintering temperature. From the above results it is obvious that the compound synthesized via sol-gel has exhibited a large dielectric constant of 18,000 while SSR and molten-salt methods showed approximately 14,000. Here it is worth to notice that the synthesis technique, sintering temperatures and the grain size play a major role in deciding dielectric constant of ferroelectrics. Further another important point to be noticed is contrary to the conversional viewpoint that permittivity decreases with decrease in grain size below μm range is proved wrong [6,8]. The present results where all the compounds grain size is less than 100 nm have exhibited permittivity above 14,000. The high dielectric constant is mainly attributed to the grain size (nanometer range) as the number of grains and grain boundaries are high; resulting in high Lorentz fields [20].

4.7. Diffuse phase transition (DPT)

Ferroelectric materials execute Curie-Weiss law in para electric

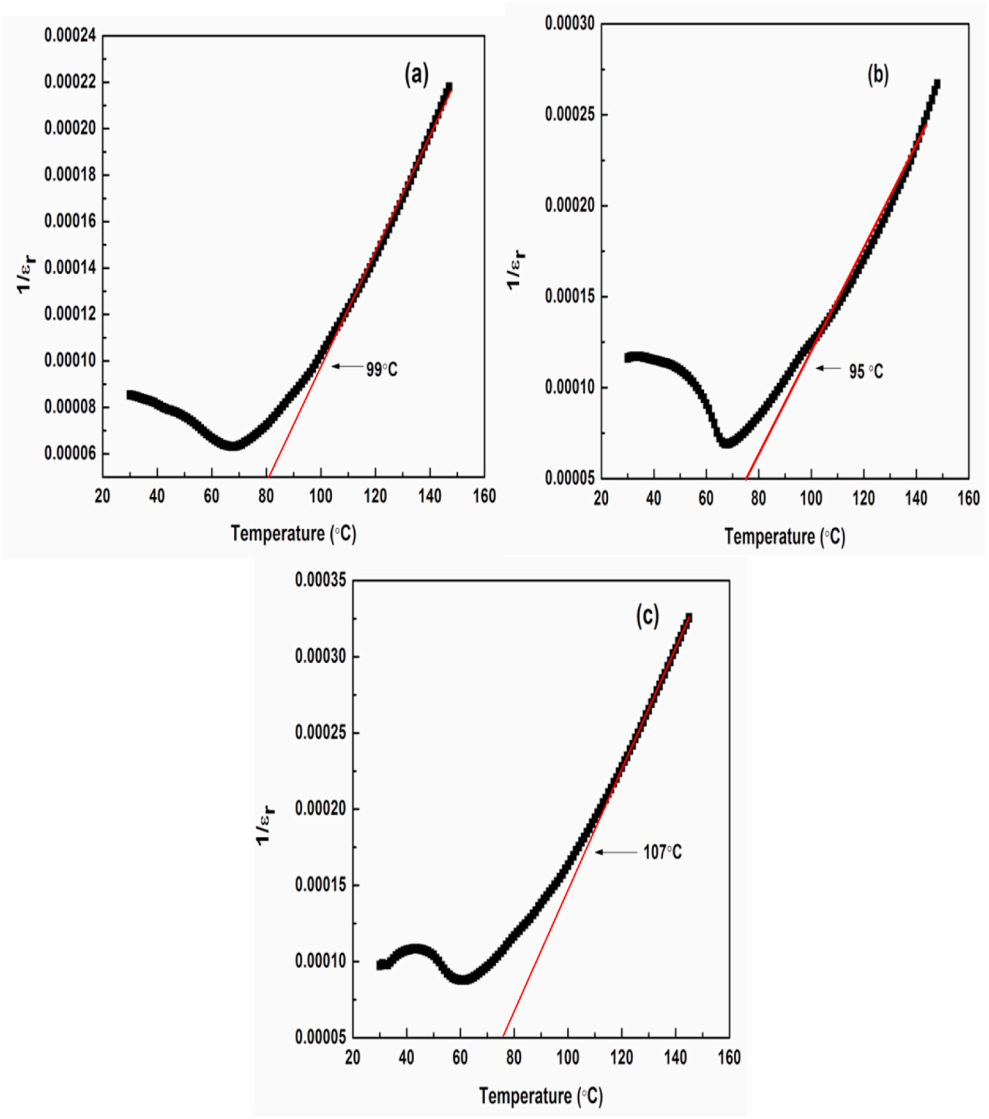

Fig. 8. Burns temperature of BCT-BST. (a) SSR (b) sol-gel method and (c) molten-salt method.

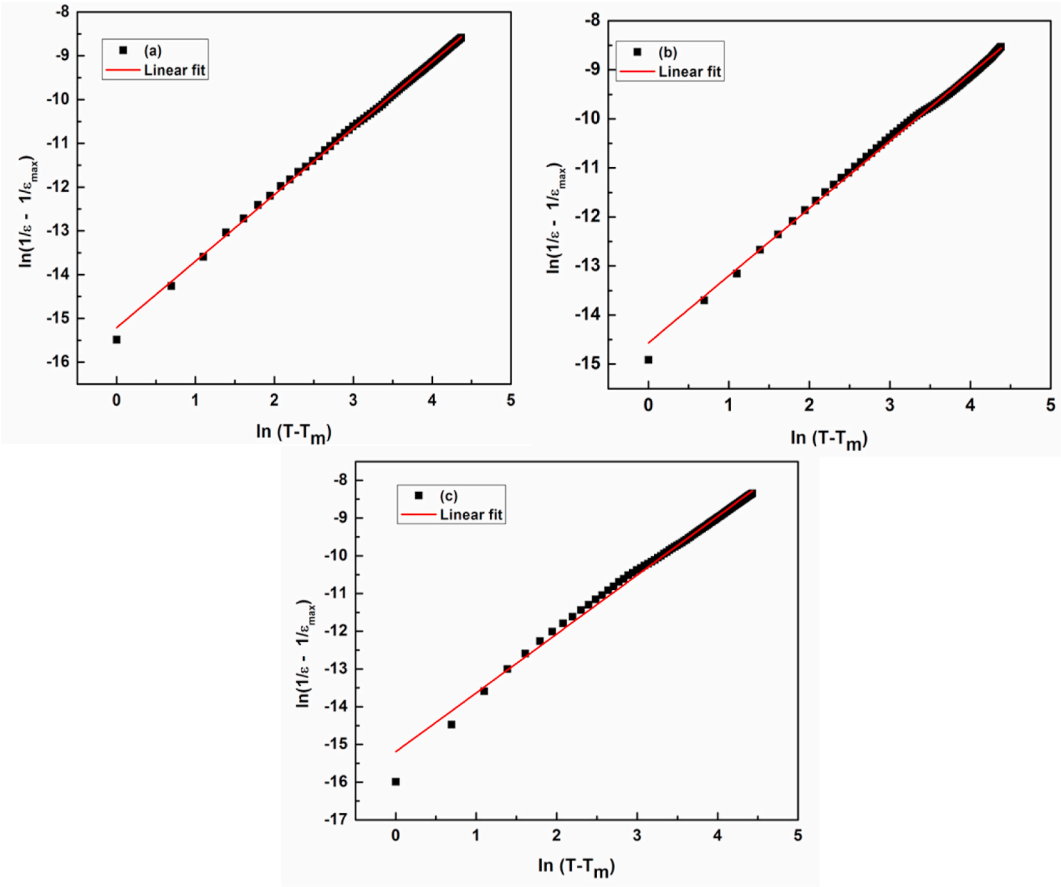

Fig. 9. Linear fitted plot for in ($T-T_m$) and in ($1/\varepsilon - 1/\varepsilon_{max}$) of BCT-BST (a) SSR, (b) sol-gel method and (c) molten-salt method.

Table 3
Degree of relaxation (γ) Curie- Weiss Constant (C) Burns Temperature (T_B) and ΔT_m Calculated from Diffuse Phase Transition Plot at 10 kHz.

Synthesis methods	Dielectric Constant (ε_{max})	Degree of relaxation (γ)	Curie- Weiss Constant (C)	Burns Temperature (T_B)	On set of Curie-Weiss law (ΔT_m)	Conductivity temperature at 0.1 kHz (T_s)
SSR	13,112	1.52	15.214	99	28	121 °C
Sol-gel	14,478	1.37	14.567	95	24	135 °C
Molten salt	11,390	1.56	15.193	107	41	123 °C

phase. The below relation is Curie Weiss law (2)

$$\frac{1}{\varepsilon} = \frac{T - T_C}{C} \quad (2)$$

Where ε is the dielectric constant, T is the absolute temperature, T_c is the Curie transition temperature and C is the Curie-Weiss constant [21]. Fig. 8 shows the $1/\varepsilon$ with the temperature at 10 kHz. The curve is fitted to the Curie-Weiss law the deviation from the line is Burns temperature (T_B) or Curie-Weiss temperature. The compounds follow Curie-Weiss law in the temperature after the transition temperature. Normally the deviation is observed in the relaxor ferroelectric materials due to polar cluster. This is the evidence for BCT-BST ceramics are relaxor ferroelectric materials. From Fig. 8 resulted the Curie-Weiss behavior (ΔT_m) or on set of Curie-Weiss law is calculated using the relation (3).

$$\Delta T_m = T_B - T_C \quad (3)$$

Fig. 9 shows the modified Curie-Weiss law is used to explain the dielectric behavior of complex ferroelectric with DPT in relation (4).

$$\frac{1}{\varepsilon} - \frac{1}{\varepsilon_{max}} = \frac{(T - T_m)^{\gamma}}{C} \quad (4)$$

Where, ε_{max} is the maximum dielectric constant at T_C point and γ is the degree of diffusion constant [22]. If the value of γ is 1 the material illustrates classical ferroelectric phase transition and materials follow normal Curie-Weiss law. If γ value is 2, the materials are considered as DPT materials. The calculated values are tabulated in Table 3. The values are lie in the range of 1.37–1.56 indicating once again that BCT-BST composite exhibit DPT [23,24]. The difference between the T_B and T_C denotes degree of diffuseness of the diffuse phase transition (DPT).

4.8. Conductivity property

Fig. 10 shows the AC conduction with 1000/T at different frequencies. It once again proves the transition temperature of BCT-BST with a depression at the transition point. From room temperature to transition temperature the conduction is found to be independent of temperature. After transition temperature the conductivity decreases. It confirms the metallic nature of the materials and all the methods of preparation exhibited similar behavior after transition temperature point [25]. At higher temperatures of about (T_s) 120 °C and greater, the conductivity of the ceramics shows a semiconducting behavior. It is also

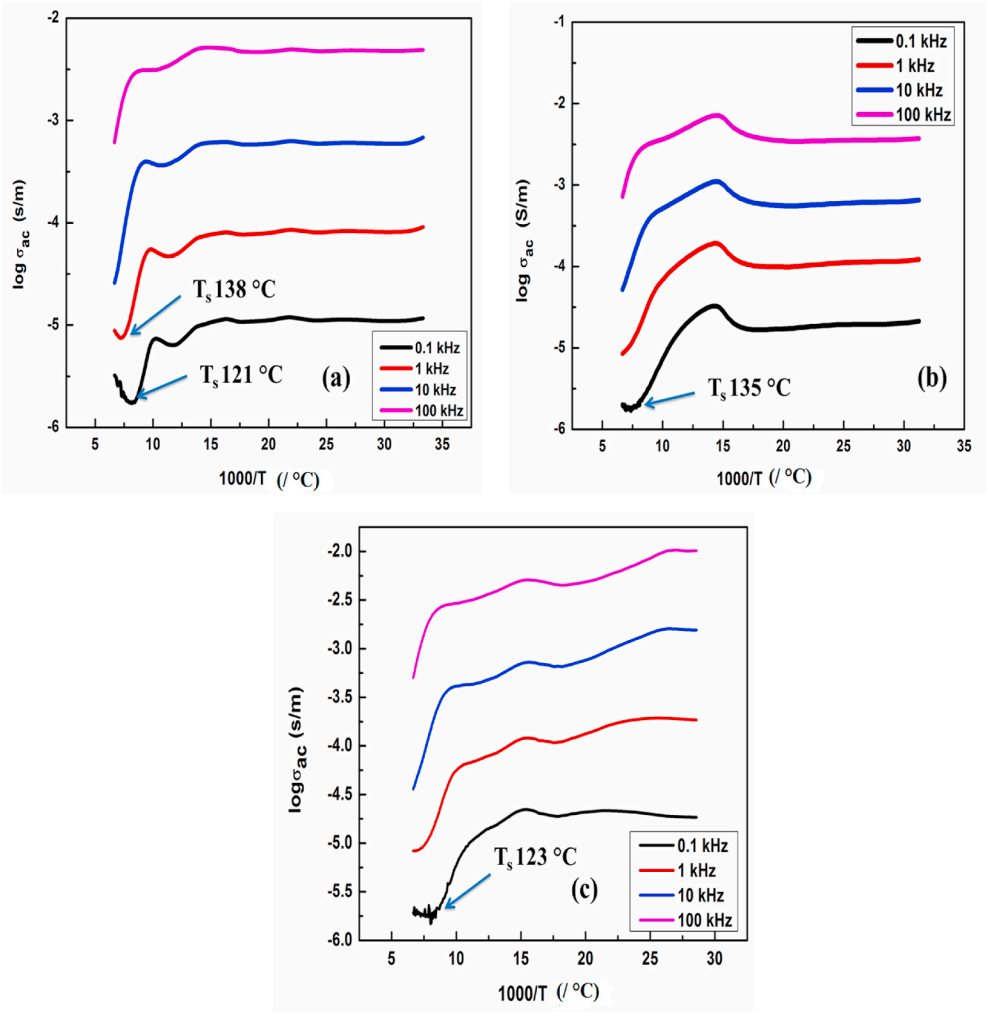

Fig. 10. Temperature with AC conductivity at Selected Frequency (a) SSR (b) Sol-Gel Method and (c) Molten-Salt Method.

noticed that as the frequency increases, T_s shifts towards higher temperatures. Further in polycrystalline materials conduction is generally by hopping mechanism. Band-like conduction mechanism is expected in either large or small polaron hopping model. However, as the frequency increases ac conductivity decreases for large polaron while it increases for small polaron hopping mechanism. From Fig. 10 it is evident that as the frequency increases conductivity is found to increase suggesting small polaron hopping mechanism of conduction. However, in depth understanding of conduction mechanism requires further experimentation and computation.

4.9. Ferroelectric study

The prepared pellet samples are poled at 1 kV/cm using DC poling unit at room temperature for 30 min. The sample is immersed in silicon oil. The P-E loop tracer is connected to a temperature controller. The poled samples are used for P-E measurements. The P-E loop at different temperatures, is shown in Fig. 11. From figure it is clear that the hysteresis loops are well developed and are saturated. Irrespective of the synthesis technique all the samples exhibit a saturation polarization approximately 8 μC/cm^2. At room temperature, the coercive field is less than 0.5 kV/cm for SSR and sol gel samples while it is slightly higher 3 kV/cm for the sample prepared by molten salt technique. The low coercive field at room temperature is also an evidence of the coexistence of orthorhombic and tetragonal phase. Very low values of coercive field suggest soft ferroelectric nature of the compositions. In other words, the compositions exhibit easy dipole/polarization rotation. This facilitates tuning of poling conditions and can greatly enhance the piezoelectric property. The E_c variation with temperature is shown in Fig. 12. The sharp dip in coercivity is observed at the transition temperature because the dipoles are misaligned at the transition point due to which coercive field decreases [26–30].

5. Conclusion

The BCT-BST ceramics are prepared by solid state route, sol-gel and molten-salt techniques. The ceramics are studied and compared for dielectric and ferroelectric properties. The thermal analysis of the prepared samples reveals the calcination temperature of BCT-BST. It is noticed that SSR methods requires higher calcination temperature (>1200 °C) than sol-gel and molten salt technique (≅1000 °C). Prepared samples possess cubic crystal structure confirmed by X-ray powder diffraction and crystallite size is found to be 50 nm for SSR method, 35 nm for a sol-gel method and 34 nm for the molten-salt method. The metal-oxide bond formation of BCT-BST is confirmed from Fourier Transform Infra-red analysis. BCT-BST samples average particle size from Scanning Electron Microscope found to be in 1 μm, 45 nm and 32 nm for SSR, molten salt method and sol-gel methods respectively. The dielectric constant with temperature at different frequency revealed the large dielectric constant of 16,000. Compared to all the methods the very large dielectric constant was found to be 18,000 in the sol-gel method. Diffuse phase transition of the ceramic is confirmed by

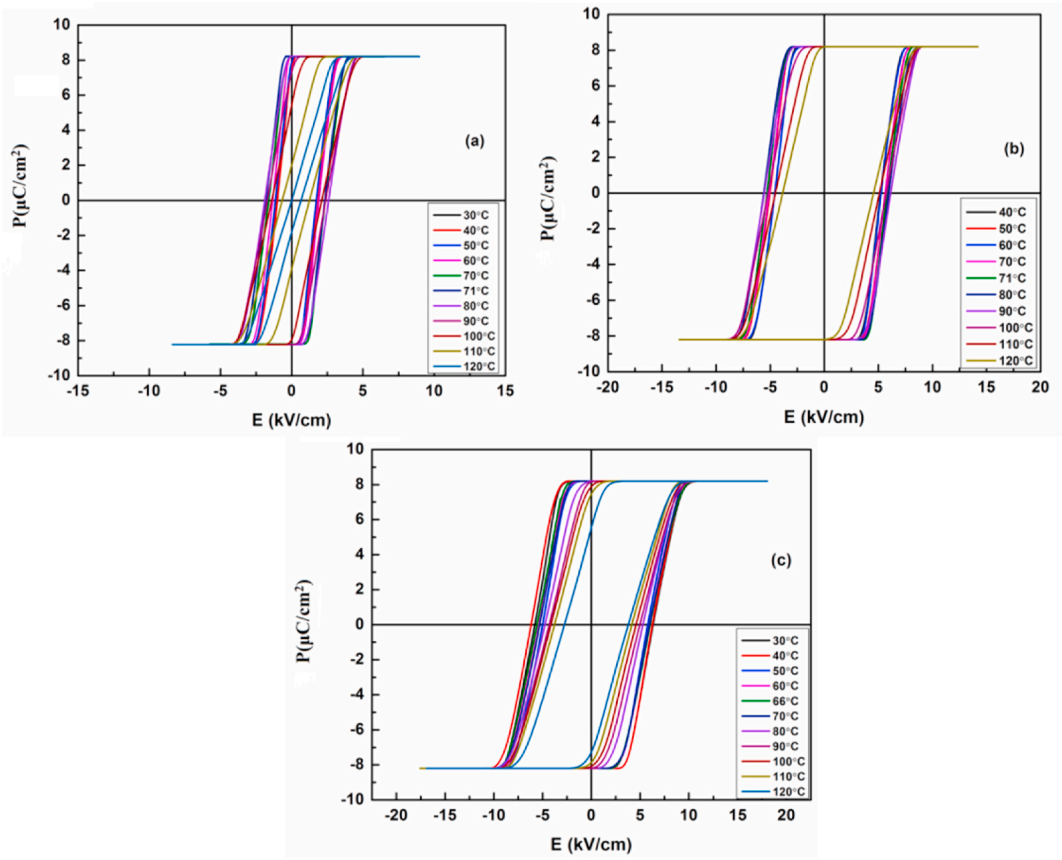

Fig. 11. P–E loop for BCT-BST at Different Temperature (a) SSR (b) Sol-Gel Method and (c) Molten-Salt Method.

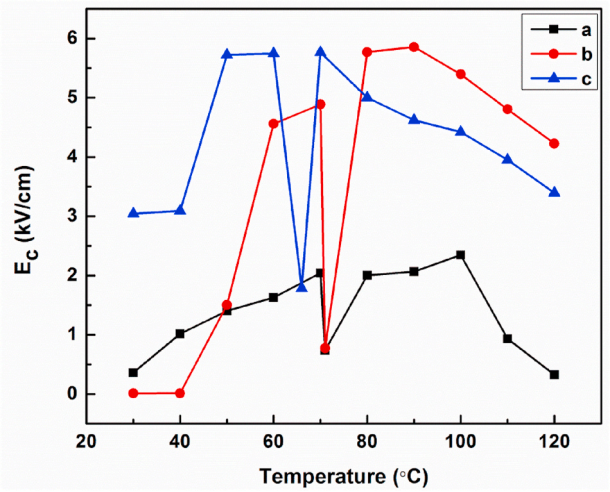

Fig. 12. Temperature with coercivity (a) SSR (b) sol-gel method and (c) molten-salt method.

applying Curie-Weiss law in the paraelectric region. The AC conductivity of samples confirms the metallic nature of the materials after the transition point and semiconductor behavior at high temperatures. The ferroelectric property confirms that BCT-BST is soft and a ferroelectric to paraelectric transition temperature exactly matches with that obtained from dielectric studies.

CRediT author contribution statement

C. Pavithra: Data curation, Writing - original draft, preparation, Visualization, Investigation. **W. Madhuri:** Supervision, Validation, Writing - review & editing. **S. RoopasKiran:** Conceptualization, Methodology, Software.

Declaration of competing interest

The authors declare that they have no known competing financial interests or personal relationships that could have appeared to influence the work reported in this paper.

References

[1] S. Lu, Z. Xu, R. Zuo, Comparative study of the effect of domain structures on piezoelectric properties in three typical Pb-free piezoceramics, Ceram. Int. 40 (2014) 13565–13571, https://doi.org/10.1016/j.ceramint.2014.05.070.

[2] J. Rani, K.L. Yadav, S. Prakash, Structural, dielectric and optical properties of sol–gel synthesized 0.55Ba($Zr_{0.2}Ti_{0.8}$)$O_3$0.45($Ba_{0.7}Ca_{0.3}$)TiO_3 ceramic, Appl. Phys. Mater. Sci. Process 45 (2014) 1131–1137, https://doi.org/10.1007/s00339-014-8482-4.

[3] Y. Sun, Y. Chang, J. Wu, X. Wang, S. Zhang, R. Wang, B. Yang, W. Cao, Domain structures and piezoelectric properties of low-temperature sintered ($Ba_{0.95}Ca_{0.05}$)($Ti_{0.94}Sn_{0.06}$)O_3 ceramics with CuO additive, Mater. Lett. 177 (2016) 128–131, https://doi.org/10.1016/j.matlet.2016.04.125.

[4] Z. Zhu, X. Guo, Z. Wang, G. Yuan, Y. Wang, Z. Cai, L. Chen, J. Chen, Y. Zhang, Z. Liu, Ferroelectric and piezoelectric properties of Ba ($Ti_{0.89}Sn_{0.11}$)O_3 thin films prepared by sol – gel method, Chem. Phys. Lett. 638 (2015) 168–172, https://doi.org/10.1016/j.cplett.2015.08.033.

[5] H. Han, D. Ghosh, J.L. Jones, J.C. Nino, Colossal permittivity in microwave-sintered barium titanate and effect of annealing on dielectric properties, J. Am. Ceram. Soc. 490 (2013) 485–490, https://doi.org/10.1111/jace.12051.

[6] Y. Tan, J. Zhang, Y. Wu, C. Wang, V. Koval, B. Shi, H. Ye, R. Mckinnon, G. Viola, H. Yan, Unfolding grain size effects in barium titanate ferroelectric ceramics, Sci. Rep. 5 (2015) 15–21, https://doi.org/10.1038/srep09953.

[7] Weiwei Mao, Qifu Yao, Yingfang Fan, Yile Wang, Xingfu Wang, Yong Pu, Xing'ao Li, Combined experimental and theoretical investigation on modulation of multiferroic properties in BiFeO3 ceramics induced by Dy and transition metals co-doping, J. Alloys Compd. 784 (2019) 117–124, https://doi.org/10.1016/j.jallcom.2018.12.381.

[8] L. Zhu, B. Zhang, L. Zhao, S. Li, Y. Zhou, X. Shi, N. Wang, Large piezoelectric effect of (Ba,Ca)TiO_3 – x Ba(Sn,Ti)O_3 lead-free ceramics, J. Eur. Ceram. 36 (2016) 1017–1024, https://doi.org/10.1016/j.jeurceramsoc.2015.11.039.

[9] J.P. Praveen, K. Kumar, A.R. James, T. Karthik, S. Asthana, D. Das, Large piezoelectric strain observed in sol e gel derived BZT - BCT ceramics, Curr. Appl. Phys. 14 (2014) 396–402, https://doi.org/10.1016/j.cap.2013.12.026.

[10] V.A. Online, Z. Wang, K. Zhao, X. Guo, W. Sun, H. Jiang, X. Han, X. Tao, Z. Cheng, H. Zhao, H. Kimura, G. Yuan, J. Yin, Z. Liu, Crystallization, phase evolution and ferroelectric properties of sol–gel-synthesized Ba($Ti_{0.8}Zr_{0.2}$)O_3– x($Ba_{0.7}Ca_{0.3}$)TiO_3 thin film, J. Mater. Chem. C. 1 (2013) 522–530, https://doi.org/10.1039/c2tc00020b.

[11] C. Zhao, H. Wang, J. Xiong, J. Wu, Composition-driven phase boundary and electrical properties in ($Ba_{0.94}Ca_{0.06}$)($Ti_{1-x}M_x$)O_3 (M = Sn, Hf, Zr) lead-free ceramics, Dalton Trans. 45 (2016) 6466–6480, https://doi.org/10.1039/c5dt04891e.

[12] Piaojie Xue, Yang Hu, Weiren Xia, Heng Wu, Xinhua Zhu, Molten-salt synthesis of BaTiO3 powders and their atomic-scale structural characterization, J. Alloys Compd. 695 (2017) 2870–2877, https://doi.org/10.1016/j.jallcom.2016.11.395.

[13] A. Manohar, C. Krishnamoorthi, Site selective Cu^{2+} substitution in single crystal Fe_3O_4 biocompatible nanospheres by solvothermal reflux method, J. Cryst. Growth J. 473 (2017) 66–74, https://doi.org/10.1016/j.jcrysgro.2017.05.013.

[14] C. Pavithra, W. Madhuri, Electrical and magnetic properties of $NiTiO_3$ nanoparticles synthesized by the sol-gel synthesis method and microwave sintering, Mater. Chem. Phys. 211 (2018) 144–149, https://doi.org/10.1016/j.matchemphys.2018.02.019.

[15] A.Manohar, C. Krishnamoorthi, Structural, Raman, Magnetic and Other Properties of Co- Substituted - $ZnFe_2O_4$ Nanocrystals Synthesized by Solvothermal Reflux Method, (2017). doi:10.1007/s10854-017-7967-2.

[16] Z. Zhu, X. Guo, Z. Wang, G. Yuan, Y. Wang, Z. Cai, L. Chen, J. Chen, Y. Zhang, Z. Liu, Ferroelectric and piezoelectric properties of Ba ($Ti_{0.89}Sn_{0.11}$)O_3 thin films prepared by sol – gel method, Chem. Phys. Lett. 638 (2015) 168–172, https://doi.org/10.1016/j.cplett.2015.08.033.

[17] C. Basavaraja, Y.M. Choi, H.T. Park, D.S. Huh, L.J. Wook, M. Revanasiddappa, S. C. Raghavendra, S. Khasim, T.K. Vishnuvardhan, Preparation , characterization and low frequency a . c . Conduction of polypyrrole-lead titanate composites, Bull. Kor. Chem. Soc. 28 (2007) 1104–1108.

[18] C. Pavithra, W. Madhuri, S. Roopas Kiran, N. Arunai Nambi Raj, K.V. Siva Kumar, Elastic and anelastic behavior of microwave sintered BCT-BST ceramics, Int. J. Eng. Adv. Technol. (2019) 9, https://doi.org/10.35940/ijeat.A1071.1291S319.

[19] A. Manohar, C. Krishnamoorthi, Low Curie-transition temperature and superparamagnetic nature of Fe_3O_4 nanoparticles prepared by colloidal nanocrystal synthesis, Mater. Chem. Phys. 192 (2017) 235–243, https://doi.org/10.1016/j.matchemphys.2017.01.039.

[20] W. Madhuril, C. Pavithra, Dielectric , piezo and ferroelectric properties of microwave sintered $PbTiO_3$ synthesized by sol – gel method, J. Sol. Gel Sci. Technol. (2017), https://doi.org/10.1007/s10971-017-4565-y.

[21] V. Sreenivas, D.K. Pradhan, W. Pe, Structure , dielectric tunability , thermal stability and diffuse phase transition behavior of lead free BZT – BCT ceramic capacitors, J. Phys. Chem. Solid. 74 (2013) 466–475, https://doi.org/10.1016/j.jpcs.2012.11.012.

[22] V.S. Puli, D.K. Pradhan, B.C. Riggs, Synthesis and characterization of lead-free ternary component BST – BCT – BZT ceramic capacitors, J. Adv. Dielectr. 4 (2014) 1450014–1450022, https://doi.org/10.1142/S2010135X14500143.

[23] D. Zhang, Y. Gan, T. Chen, S. Yang, Y. Zhang, Phase transition and enhanced electrical properties in0.725$BiFeO_3$-0.275$Ba_{0.85}Ca_{0.15}Ti_{0.9}Zr_{0.1}$â^'xSnx$O_3$ multiferroic ceramics, J. Alloys Compd. 637 (2015) 137–142, https://doi.org/10.1016/j.jallcom.2015.02.127.

[24] J. Wang, X. Zhang, J. Zhang, H. Li, Z. Li, Dielectric and piezoelectric properties of (1-x)$Ba_{0.7}Sr_{0.3}TiO_3$-x$Ba_{0.7}Ca_{0.3}TiO_3$ perovskites, J. Phys. Chem. Solid. 73 (2012) 957–960, https://doi.org/10.1016/j.jpcs.2012.03.004.

[25] R. Gupta, S. Das, T.P. Sinha, K.K. Bamzai, Effect of cadmium doping on electrical properties of lead nickel niobate – lead zirconate titanate [$Pb_{1.0}(Ni_{0.167}Nb_{0.333}Zr_{0.155}Ti_{0.345})O_3$] ceramics, Ceram. Int. 41 (2015) 13241–13249, https://doi.org/10.1016/j.ceramint.2015.07.103.

[26] V.S. Puli, R. Picchini, C. Orozco, C.V. Ramana, Controlled and enhanced dielectric properties of high-titanium containing $Li_xTi_{0.1}Ni_{1-x}O$ via chemical, Chem. Phys. Lett. 649 (2016) 115–118, https://doi.org/10.1016/j.cplett.2016.01.054.

[27] S. Hunpratub, S. Phokha, S. Maensiri, P. Chindaprasirt, Dielectric and piezoelectric properties of lead-free $Ba_{0.85}Ca_{0.15}Ti_{0.9-x}Zr_{0.1}Cu_xO_3$ ceramics synthesized by a hydrothermal method, Appl. Surf. Sci. 369 (2016) 334–340, https://doi.org/10.1016/j.apsusc.2016.01.273.

[28] N. Ma, B. Zhang, W. Yang, D. Guo, Phase structure and nano-domain in high performance of $BaTiO_3$ piezoelectric ceramics, J. Eur. Ceram. Soc. 32 (2012) 1059–1066, https://doi.org/10.1016/j.jeurceramsoc.2011.11.014.

[29] X. Liu, M. Zhu, Z. Chen, B. Fang, J. Ding, X. Zhao, H. Xu, Structure and electrical properties of Li-doped $BaTiO_3$–$CaTiO_3$–$BaZrO_3$ lead-free ceramics prepared by citrate method, J. Alloys Compd. J. 613 (2014) 219–225, https://doi.org/10.1016/j.jallcom.2014.06.046.

[30] Y.G. Yao, C. Zhou, D.C. Lv, D. Wang, H.J. Wu, Y.D. Yang, X.B. Ren, Large piezoelectricity and dielectric permittivity in $BaTiO_3$–x$BaSnO_3$ system: the role of phase coexisting, Europhys. Lett. 98 (2) (2012) 27008.